A Topographic–Rossby Mode Resonance over the Iceland–Faeroe Ridge

ARTHUR J. MILLER

Scripps Institution of Oceanography, La Jolla, California

PIERRE F. J. LERMUSIAUX

Harvard University, Cambridge, Massachusetts

PIERRE-MARIE POULAIN

Naval Postgraduate School, Monterey, California

(Manuscript received 7 September 1995, in final form 31 May 1996)

ABSTRACT

An array of current meter moorings along 12°W on the southern side of the Iceland–Faeroe Ridge reveals a narrowband barotropic oscillation with period 1.8 days in spectra of velocity. The signal is coherent over at least 55-km scales and propagates phase with shallow water on the right (toward the northwest). Velocity ellipses tend to be elongated (crossing contours of f/H) and rotate anticyclonically. Solutions of the rigid-lid barotropic shallow-water equations predict the occurrence of a topographic–Rossby normal mode on the south side of the ridge with spatial scales exceeding 250 km and with intrinsic period near 1.84 days. This fundamental mode of the south side of the ridge has predicted spatial structure, phase propagation, and velocity ellipses consistent with the observed oscillation. The frictional amplitude e-folding decay time for this normal mode is estimated from the observations to be 13 days. The observed ocean currents are significantly coherent with zonal wind stress fluctuations (but not with wind stress curl) in the relevant period band, which indicates the oscillation is wind forced. This appears to be the first clear evidence of a stochastically forced resonant barotropic topographic–Rossby normal mode in the ocean.

1. Introduction

The energetic frontal current between Iceland and the Faeroe Islands is known to generate mesoscale eddies with short timescales (a few days) and short length scales (10–20 km). Typically, one finds that moorings placed 25 km apart show little or no correlation among horizontal currents in the mesoscale band, at least when based on correlation analysis among time series from current meter moorings (e.g., Hopkins 1991; Perkins 1992; Niiler et al. 1992) and surface drifters (Poulain et al. 1996).

It was therefore surprising to discover significant peaks, at 1.8-day periods, in coherence spectra among current meter moorings spaced up to 55 km apart along the southern flank of the Iceland–Faeroe Ridge (IFR). These coherency peaks were associated with significant narrowband peaks in the power spectra of barotropic currents (4 cm s^{-1} rms).

We suspected that the peaks were the signature of a resonant barotropic topographic–Rossby normal mode trapped to the IFR, so we commenced an extensive analysis of the data that we report here (§2). We also have applied a theoretical model of barotropic normal modes based on the rigid-lid shallow-water equations (Miller 1986), which predicts that the fundamental barotropic topographic–Rossby mode of the south side of the IFR has a period near 1.8 days (§3). This combination of data analysis and normal mode solutions provides compelling evidence that we have observed a resonant stochastically forced barotropic topographic–Rossby normal mode, apparently for the first time (§4a). A direct estimate of the oceanic frictional damping time then follows (§4b). Significant coherency with wind stress indicates the normal mode is atmospherically driven (§4c).

2. Data analysis

Nine current meter moorings situated along 12°W (Fig. 1) were deployed from October 1992 through August 1993 over the IFR. A typical mooring had three current meters, one near the surface (80 m), one at middepth (200 m), and one near the bottom (300 m), though several records were lost or had partial returns.

Corresponding author address: Dr. Arthur J. Miller, Scripps Institution of Oceanography, University of California, La Jolla, CA 92093-0224.
E-mail: ajmiller@ucsd.edu

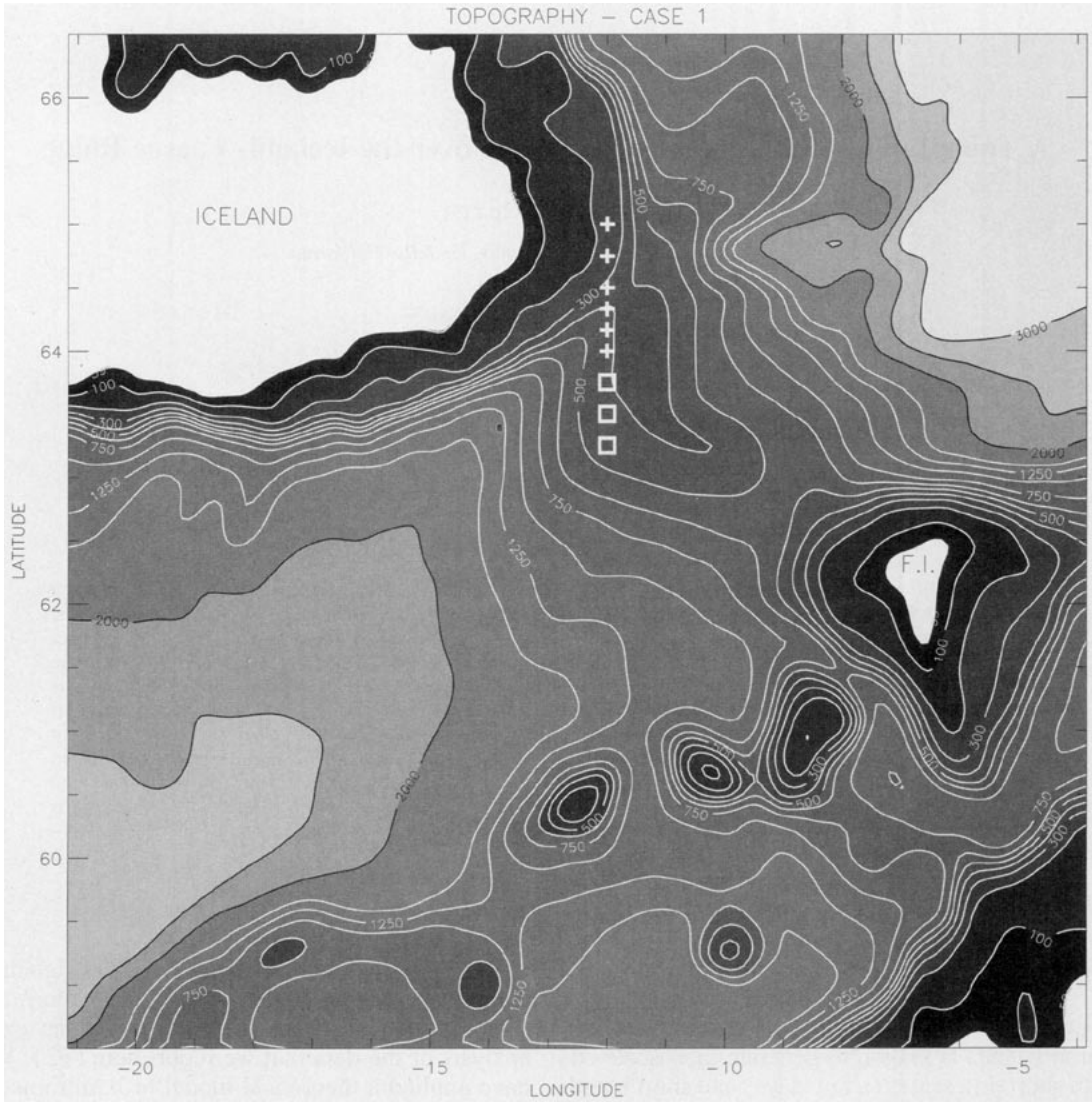

FIG. 1. Topography of the region around Iceland and the Faeroe Islands (used for model case 1), smoothed with a five-point (2–4–5–4–2) grid-scale filter. The array of nine current meter moorings (along 12°W) is indicated by the symbols; boxes indicate the three moorings discussed in the text that reveal the 1.8-day resonance, while + indicate the additional moorings. The irregular contour intervals are marked, and depths shallower than 50 m are shaded white. The axes are labeled as longitude and latitude for convenience of viewing, but the longitudinal labeling is accurate only along 62.5°N because the 5.55-km grid is locally Cartesian based on linear distance from the central point (62.5°N, 12.5°W).

The instruments used were Aanderaa RCM-7 vector-averaging current meters equipped with a rotor and magnetic compass to measure current speed and direction, and with a pressure sensor, a thermistor, and an inductive conductivity cell. The data, originally sampled at hourly intervals, were low-pass filtered with a cutoff period of 36 h (−3 dB reduction at 36 h and −49 dB reduction at 27 h) to suppress strong tidal and inertial signals.

Power spectra were computed of horizontal velocity ($\mathbf{u}$), its components (u, v), temperature T, and salinity S by dividing the time series into 30-day 50% overlapping segments, Fourier transforming the relevant quantity, averaging the spectral estimates, and estimating the 95% confidence limits under classical assumptions (Bendat and Piersol 1986). The most robust subinertial signal was a peak, with a period near 1.8 days, in power spectra of velocity at all eight current meters in moorings 1 (63.25°N, 12°W), 2 (63.5°N, 12°W), and 3 (63.75°N, 12°W). For example, Fig. 2 shows rotary spectra from mooring 1 at 80 m, 200 m, and 300 m. The narrowband peaks in the anticyclonic current is well above (95%) the red background. The power in that period band indicates 4–5 cm s^{-1} rms velocity. The energy in the spectral peaks at each depth is nearly equal, with power varying by less than 40% from 80

m to 300 m depth, suggesting a nearly barotropic signal. No corresponding peaks appear in temperature or salinity time series, consistent with barotropic motion.

Coherence spectra among adjacent, as well as distant, moorings were also calculated for velocity and temperature time series using 30-day 50%-overlapping records as done for the power spectra. Cross-spectra among currents at individual moorings indicate the 1.8-day signal is, indeed, nearly barotropic. For example, Fig. 3 (open circles) shows the coherence magnitude is 0.97 between meridional currents at 80 and 300 m on mooring 1, while the coherence phase is nearly zero (−4°). No coherency was found in the frequency band of interest between velocity and temperature time series, again consistent with nearly pure barotropic motion.

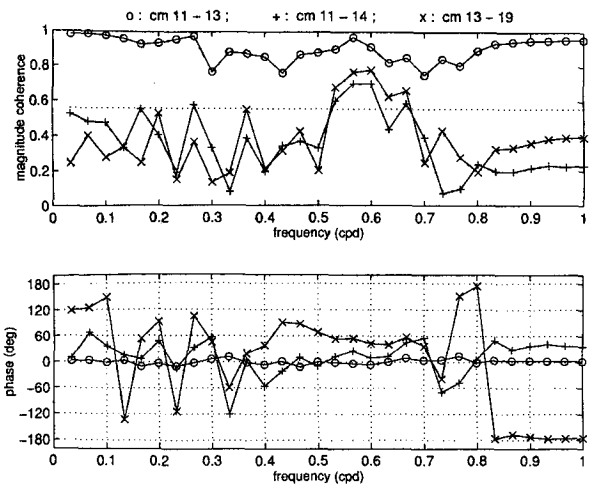

FIG. 3. Coherence spectra of meridional currents; (top) coherence magnitude, (bottom) coherence phase. Circles correspond to mooring 1 (63.25°N, 12°W) at 80 and 300 m, + correspond to 80 m at mooring 1 and mooring 2 (63.5°N, 12°W), and × correspond to 300 m at mooring 1 and mooring 3 (63.75°N, 12°W). The 95% level of significance for the coherence amplitude is indicated by the dotted line. The 95% confidence limits for coherence phase are ±25°, assuming true coherence is 0.70 with 21.6 degrees of freedom. Positive phase indicates that the first variable leads the second.

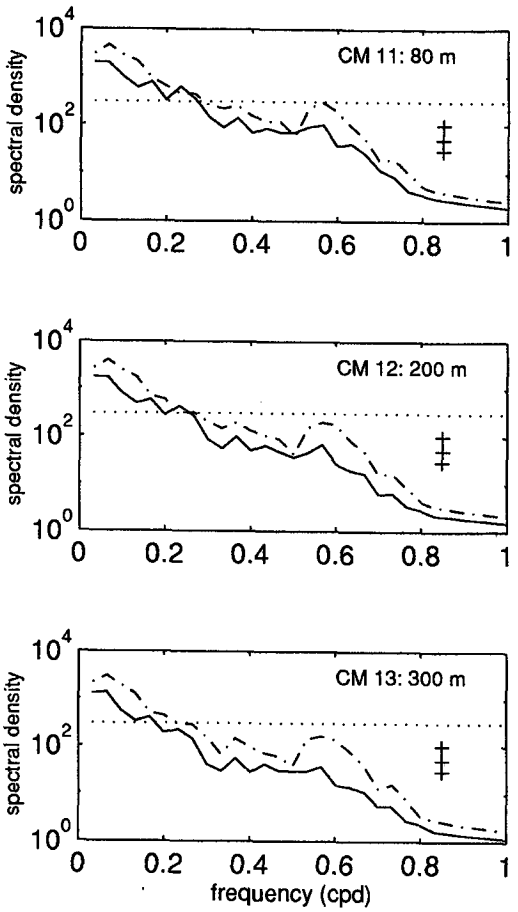

FIG. 2. Rotary power spectra of horizontal currents [(cm s^{-1})^2/cpd] from mooring 1 (63.25°N, 12°W) at 80-m (top), 200-m (middle), and 300-m (bottom) nominal depths. Cyclonic is solid, anticyclonic is dash–dotted, and 95% confidence limits (based on 21.6 degrees of freedom) are indicated by the horizontal ticks on the short vertical line. The dotted line above the spectral peak in each plot is a reference amplitude [300 (cm s^{-1})^2/cpd] to indicate the near barotropicity of the signal.

Cross-spectra among currents at distant moorings indicate that the 1.8-day signal is coherent over at least 55-km length scales (the distance between moorings 1 and 3). For example, Fig. 3 shows that the coherence amplitude is significantly nonzero between 80-m meridional currents at moorings 1 and 2 (+) and also between 300-m meridional currents at moorings 1 and 3 (×). The coherence phase at 0.56 cpd in Fig. 3 indicates that the signal propagates with shallow water on the right, with approximately a 25° lag from mooring 1 to 2 and a 54° lag from mooring 1 to 3 (95% confidence limits on the phase are ±25° assuming the true coherence is 0.7). Zonal currents are less coherent than meridional currents among the moorings, since the 1.8-day signal tends to have a larger amplitude for the north–south velocity (as will be shown later). The 1.8-day signal[1] is not significantly coherent with the remaining six moorings (numbered 4 through 9, northward over the ridge).

Table 1 presents the coherence magnitude and phase estimates (in the 0.56-cpd frequency bin) between 200-m meridional velocity at mooring 1 and meridional and zonal velocity at each depth of moorings 1, 2, and 3. Meridional velocity at 200 m at mooring 1 was chosen as the primary input because it has greater coherence

[1] A separate 1.5-day signal was found to be coherent among only the northernmost three moorings, which we suspect to be a topographic mode trapped on the north side of the Iceland–Faeroe Ridge, but its interpretation has not yet been firmly established.

TABLE 1. Coherence magnitude (phase) between 200-m meridional velocity (v) at mooring 1 and velocity components at other moorings for the 1.8-day signal: 95% significance level of coherence magnitude is 0.55; 95% confidence limits on phase are ±25°; *** indicates no data. Positive phase indicates v-mooring 1 (200 m) leads other field.

Depth (m)	Mooring 1	Mooring 2	Mooring 3
	Meridional velocity v		
80	0.97 (1°)	0.74 (29°)	***
200	1.00 (0°)	0.75 (25°)	0.68 (49°)
300	0.99 (−3°)	0.77 (30°)	0.74 (51°)
	Zonal velocity u		
80	0.48 (111°)	0.73 (93°)	***
200	0.55 (114°)	0.73 (104°)	0.70 (146°)
300	0.65 (102°)	0.71 (113°)	0.73 (146°)

amplitude than zonal velocity and because it is isolated from Ekman layer effects, which might contaminate coherence estimates using velocity at 80 m. The table indicates that the second mooring lags the first by approximately 28° ± 25°, and the third mooring lags the first by roughly 50° ± 25°, consistent with Fig. 3. Coherence magnitude between 200-m meridional currents at mooring 1 with zonal currents at mooring 1–3 is significantly nonzero, and the coherence phase indicates that zonal currents at mooring 1 lag their meridional counterparts by roughly 100°, which is within statistical error of the expected 90° lag of anticyclonic rotation (cf. Fig. 2). We also attempted to obtain more precise estimates of the phase lag in velocity between the three moorings by using shorter records (11-day segments), which implies more degrees of freedom in the frequency band of the 1.8-day signal. However, because the coherence magnitude decreased to near 0.50 for these calculations, the phase lag estimates (a 28° lag between mooring 1 and 2 and a 44° lag between mooring 1 and 3) were bracketed by roughly the same 95% confidence limits as those of Table 1 and Fig. 3.

Empirical orthogonal functions (EOFs) were calculated for the low-passed velocity, as well as for bandpassed velocity between 0.5 and 0.65 cpd, for all nine moorings in order to obtain a clearer picture of the spatial and temporal nature of the oscillation. The two-dimensional EOF maps (both low-passed and bandpassed) of (u, v) reveal a coherent, nearly barotropic signal that is localized around the three southern moorings. For all three southern moorings, the amplitude decays by 15%–20% from 80 to 300 m. Across the three moorings, the amplitude variation within the two EOF modes is in agreement with the previously obtained lags and the quadrature of the two modes. The principal components (EOF coefficient time series) show that the oscillation is sporadically excited in time. Four times during the approximately 290-day record we find strong excitation in the EOF coefficient time series, each lasting 10 to 15 days (20 Nov–5 Dec 1992; 30 Dec 1992–14 Jan 1993; 13–23 Feb 1993; 14–24 May 1993). During these four strong excitation events, the predominant period is 1.8 days.

Velocity ellipses and velocity variance ellipses were computed for low-passed and bandpassed data for the full records as well as for segments defined by strong signals in the EOF time series. Since the mode is excited intermittently, we present only a sample of those results for time intervals defined by the four excitation events in the EOF coefficient time series. Figure 4 shows one such plot with (0.5–0.65 cpd) bandpassed velocity plotted at each of the three moorings and each of the depths available during the 8-day interval 8–15 January 1993. The important features of Fig. 4 are that the velocity ellipses are fairly well organized, that their amplitude decays by 15%–20% with depth, and that they tend to be elongated in the north–south direction and to be angled slightly toward the northeast (across f/H contours), even though the signal is obscured by other ambient motions and measurement noise. Although the ellipses at mooring 2 in Fig. 4 tend to be more circular than those at moorings 1 and 3, at other times the ellipses at mooring 2 are more northeastwardly elongated than seen in Fig. 4, while those at moorings 1 and 3 are sometimes more circular than in Fig. 4. The prevalent features of Fig. 4 are commonly observed in the bandpassed velocity ellipses during the other excitation intervals as well.

3. Normal mode solutions

The observations strongly suggest that we have identified a resonant barotropic oscillation on the southern flank of the IFR, with phase propagation in the sense of a topographic Rossby wave. We are next motivated to obtain theoretical support for the existence of the oscillation in order to explain why the wave appears at a discrete frequency (rather than over a broad band of frequencies), why the wave appears to occur only on the southern side of the IFR (it is not coherent with the moorings north of 63.75°N), why the oscillation is intermittently excited, and what can be inferred about damping.

Since the observed wave is barotropic and occurs over the steep topography of the IFR, we adapted the numerical strategy of Miller (1986) to solve for free barotropic normal modes of the rigid-lid shallow-water equations (e.g., Rhines and Bretherton 1973) over realistic relief from the ETOPO5 dataset (5-minute resolution). Commencing with the unforced, undamped, barotropic shallow-water equations in standard notation,

$$u_t - fv = -g\eta_x \tag{1a}$$

$$v_t + fu = -g\eta_y \tag{1b}$$

$$\eta_t + \nabla\cdot(H\mathbf{u}) = 0, \tag{1c}$$

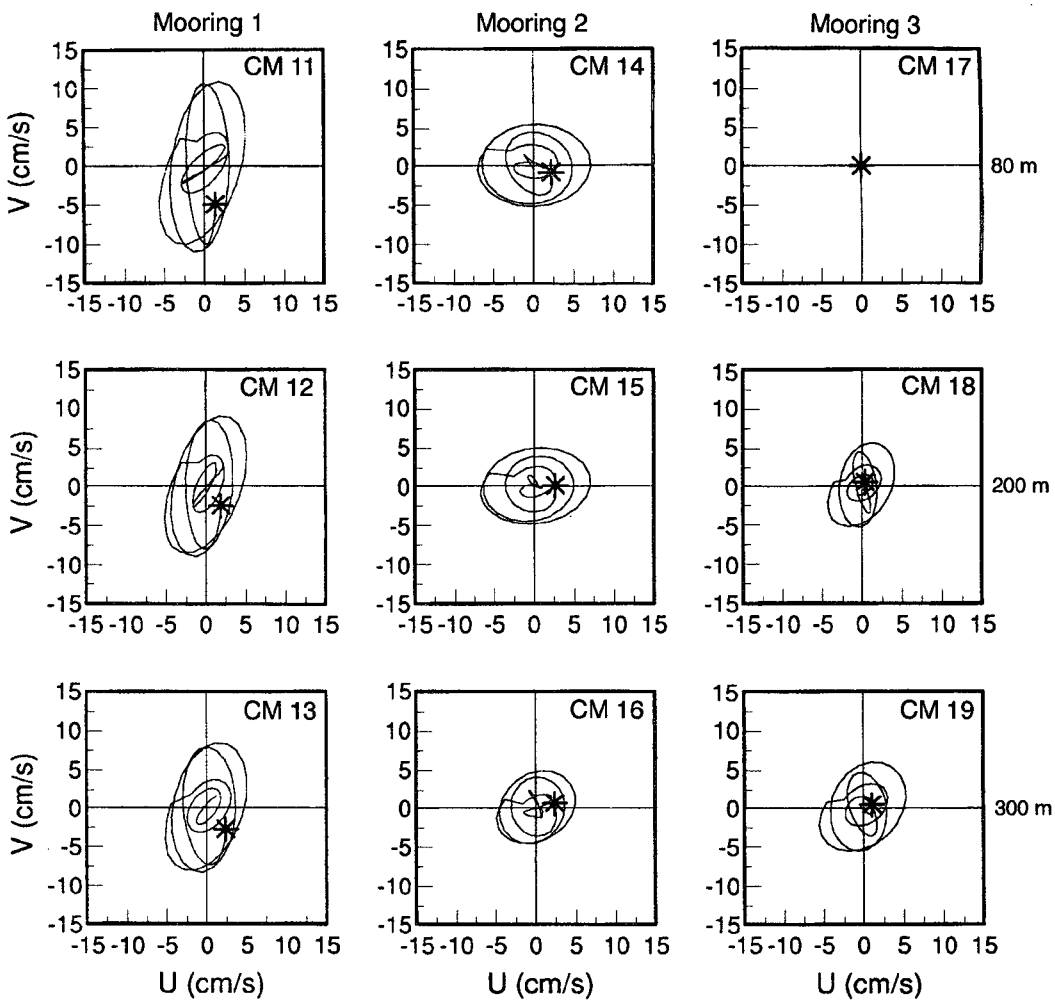

FIG. 4. Velocity ellipses during a strong mode excitation event (8–15 January 1993) for bandpassed (1.5–2.0 day periods) currents at moorings 1 (left), 2 (center), and 3 (right). Top to bottom indicates 80-m, 200-m, and 300-m nominal depths. The current meter at 80 m on mooring 3 was lost at sea. U and V correspond to eastward and northward currents. The asterisk indicates the starting velocity in each plot.

we invoke the rigid-lid approximation (appropriate for low-frequency motions), $\nabla\cdot(H\mathbf{u}) = 0$, to obtain

$$-\Psi_y = uH, \quad \Psi_x = vH \qquad (2a,b)$$

and, assuming $\Psi = \mathrm{Re}[e^{i\sigma_n t}\Phi_n(x, y)]$,

$$i\sigma_n\nabla\cdot\left(\frac{\nabla\Phi_n}{H}\right) + J\left(\Phi_n, \frac{f}{H}\right) = 0, \qquad (3)$$

where Ψ is the volume transport streamfunction, $\mathbf{u}$ is the horizontal velocity vector, η is sea level, $H(x, y)$ is the total depth of the water column, $f(y)$ is the fully varying Coriolis parameter, σ_n is the eigenfrequency, Φ_n is the streamfunction eigenmode, g is the acceleration due to gravity, $J(\cdot, \cdot)$ is the Jacobian operator, and (x, y) are the east–west and north–south coordinates. With the depth and rotation rate specified, the spherical geometry is mapped onto a square, locally Cartesian, grid for convenience. Locations where the depth of the water column is less than 50 m are set to be 50 m (including any islands in the domain). The streamfunction is set to zero along the square boundaries. Equation (3) is solved numerically via a Lanczos method (Platzman 1975) to obtain the eigenmodes and eigenfrequencies (Φ_n, σ_n). We seek solutions that are localized around topographic features and thus not influenced by reflections off the artificial boundaries.

We considered many different domains around the IFR, with resolution varying from 2.775 km (444-km square) to 5.55 km (888-km square) on a 160 × 160 horizontal grid, resulting in a 25 281 square sparse matrix self-adjoint eigenproblem. In all the domains that allowed a sufficiently large area around the southern side of the IFR (e.g., case 1 shown in Fig. 1), an ob-

vious topographic mode signature occurred with period near 1.8 days, which is the fundamental mode of the southern flank of the IFR. For example, Fig. 5 shows a solution of (3) with period 1.85 days, which occurs in the geometry of Fig. 1 (case 1). The mode structure that appears is blocked to the northwest by the sharp f/H gradients due to the shelf around Iceland and blocked to the southeast by the steep topography associated with the Faeroe Islands. The mode appears to be evanescent to the southwest, a feature also seen in results from domains that allow more area southwest of the ridge than does case 1. Phases propagate with shallow water on the right, as expected. As discussed by Miller (1986) a large-scale well-resolved mode can couple with smaller scale (often poorly resolved) modes with similar intrinsic frequencies. Thus, depending on the particular domain, we typically find a family of modes, with four or five members, each of which exhibits the basic structure seen in Fig. 5, but with slightly different period and differing structure in the regions away from the well-resolved IFR. Note that Platzman et al. (1981) also identified a topographic vorticity normal mode on the Icelandic Plateau although its period was 1.6 days in their coarsely resolved global model.

Figure 6 shows the f/H field for case 2, a domain that was selected to allow sufficient space for the existence of the fundamental mode of the south side of the ridge, to eliminate many of the surrounding topographic sites that support small-scale waves which interact with that mode, and to allow maximum resolution of the fundamental mode. A free solution of (3) for the geometry of Fig. 6 appears in Fig. 7. This mode, with period 1.84 days, is the cleanest representation of the fundamental topographic–Rossby mode of the southern side of the ridge. Five other modes (period between 1.97 and 1.75 days) exhibit weaker excitation of the spatial structure shown in Fig. 7 combined with various smaller-scale topographic waves. Discrepancies in spatial structure or period between observations and the model may be due to the neglect of stratification, the neglect of the free surface term in (3), the presence of unresolved topographic roughness in the real world, the model topography's artificial minimum depth choice of 50 m, inaccuracies in the ETOPO5 dataset, or to discretization errors. The mode is overwhelmingly controlled by the topographic variations; setting f to be constant yields only a 1 percent frequency shift to the mode pictured in Fig. 7 and little structural change.

Figure 8 shows a velocity ellipse for the theoretical normal mode of Fig. 7 at the locations of the moorings where the mode is observed, plus at mooring 4. The rotation of the currents with time is anticyclonic as observed. The ellipses are elongated northeastward across f/H contours (though not perpendicularly), as seen in Fig. 4 for the observations during an excitation event. Furthermore, the phase lag from mooring 1 to 2 is predicted to be 16° and from mooring 1 to 3 is predicted to be 40°. The observed phase lags are 28° ± 25° from mooring 1 to 2 and 50° ± 25° from 2 to 3, which agrees with the model predictions to within observational error bounds. The drop-off in mode amplitude from mooring 3 to mooring 4 seen in Fig. 8 is consistent with the lack of an identifiable signal there in the observations.

Thus, the model is able to account for all of the observed features, namely, the period, the phase propagation direction, the phase lag among the moorings, the localization around the first three moorings, and the barotropicity. It is evident that we have observed and modeled the fundamental topographic Rossby mode of the southern side of the Iceland–Faeroe Ridge.

4. Discussion

a. Observations of oceanic topographic Rossby normal modes

The solution in Fig. 7 is strong theoretical evidence that the resonant peak of the observations (Fig. 2) is a stochastically forced topographic–Rossby normal mode. It is interesting to note that there exists no other definitive observational evidence in the literature demonstrating stochastically forced resonant excitation of an oceanic barotropic topographic–Rossby normal mode trapped in both horizontal directions by f/H gradients. A normal mode (as opposed to a wave) implies that energy has saturated the spatial extent of the oscillation after multiple reflections from steep topography or turning points so that the frequency spectrum is discretized rather than continuous. Thus the extensive shelf wave literature (e.g., Brink 1991) involves oscillations trapped in only one horizontal dimension. Baroclinic Kelvin-like normal mode resonances around islands have also been observed (e.g., Luther 1995).

Narrowband peaks in a single spectrum of bottom pressure near Kerguelen Island were observed by Saint-Guily and Lamy (1988) and suggested to be resonant peaks of stochastically excited topographic normal modes, azimuthally periodic round the island. Pierini (1996) reports a single current meter spectrum in the Straight of Sicily that exhibits a peak at 3 days that corresponds to a topographic Rossby normal mode identified in his wind-forced barotropic model. A broadband peak with a period near 4 days was identified by Chave et al. (1989) in spectra of the horizontal electric field (barotropic velocity) and by Cannon and Pashinski (1990) and Cannon et al. (1991) in spectra of currents and temperature in various locales around the Juan de Fuca Ridge. This 4-day peak is clearly influenced by the sloping ridge topography (with phase propagation in the sense of a topographic Rossby wave), but it is bottom intensified (baroclinic) and has unknown spatial extent and structure. The 4-day peak may be related (via coupling) to the basin-scale coherency in tide gauges at 4–6 day periods observed by Luther (1982), which appears to be the signature of a

resonant barotropic planetary (Rossby) normal mode (or modes) of the Pacific. Miller (1989) computed the expected large-scale barotropic structure of the Pacific planetary–topographic normal modes in that period band but did not directly compare the results with Luther's (1982) sea level data.

The existence of barotropic topographic–Rossby normal modes has also been inferred in several studies of the extraordinary amplification of tidal currents observed around certain topographic features, such as the Rockall Bank and the Yermak Plateau. For example, analytical models of free barotropic vorticity modes azimuthally periodic around idealized seamounts (e.g., Huthnance 1974; Hunkins 1986) forced by ambient barotropic diurnal tidal motions (e.g., Chapman 1989) yield resonantly amplified currents for realistic parameter choices.

b. *Damping of the 1.8-day mode*

If we assume a single normal mode explains the observed peaks at 1.8 days in the current meter spectra, we can obtain an estimate of the damping timescale of the normal mode. Assuming the response is proportional to a decaying sinusoid, $\Psi \sim e^{-t/T_d}$, the decay timescale $T_d = (\Delta f_{1/2})^{-1}$, where $\Delta f_{1/2}$ is the

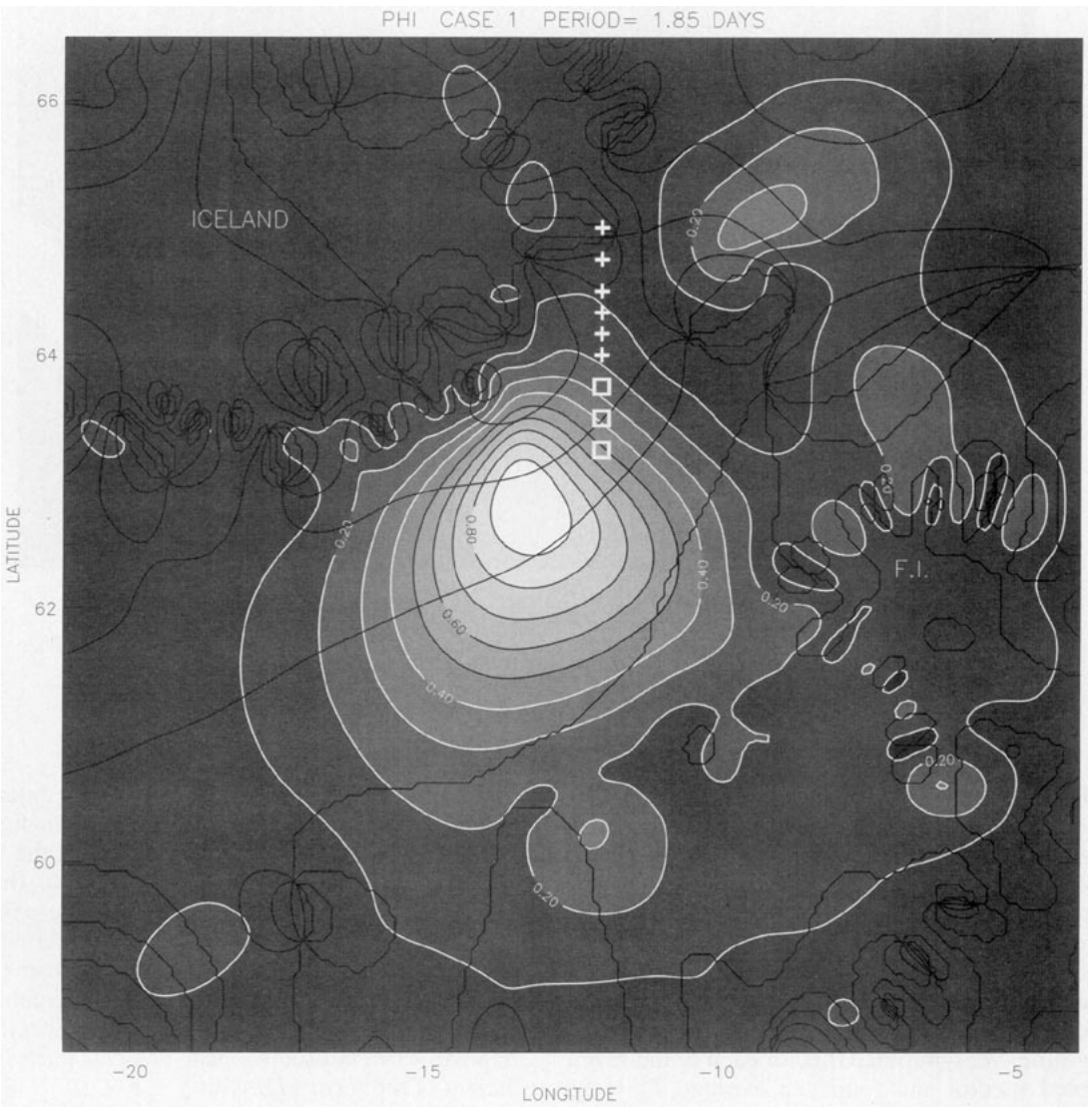

FIG. 5. Solution to (3) with period 1.85 days for the geometry of case 1 shown in Fig. 1. Volume transport streamfunction is plotted (shaded contours amplitude, heavy lines phase in $\pi/4$ intervals). Grid resolution is 5.55 km. Note that other domains, which allow more area southwest of the ridge, yield similar normal mode spatial structure (lateral extension and amplitude) and intrinsic frequency.

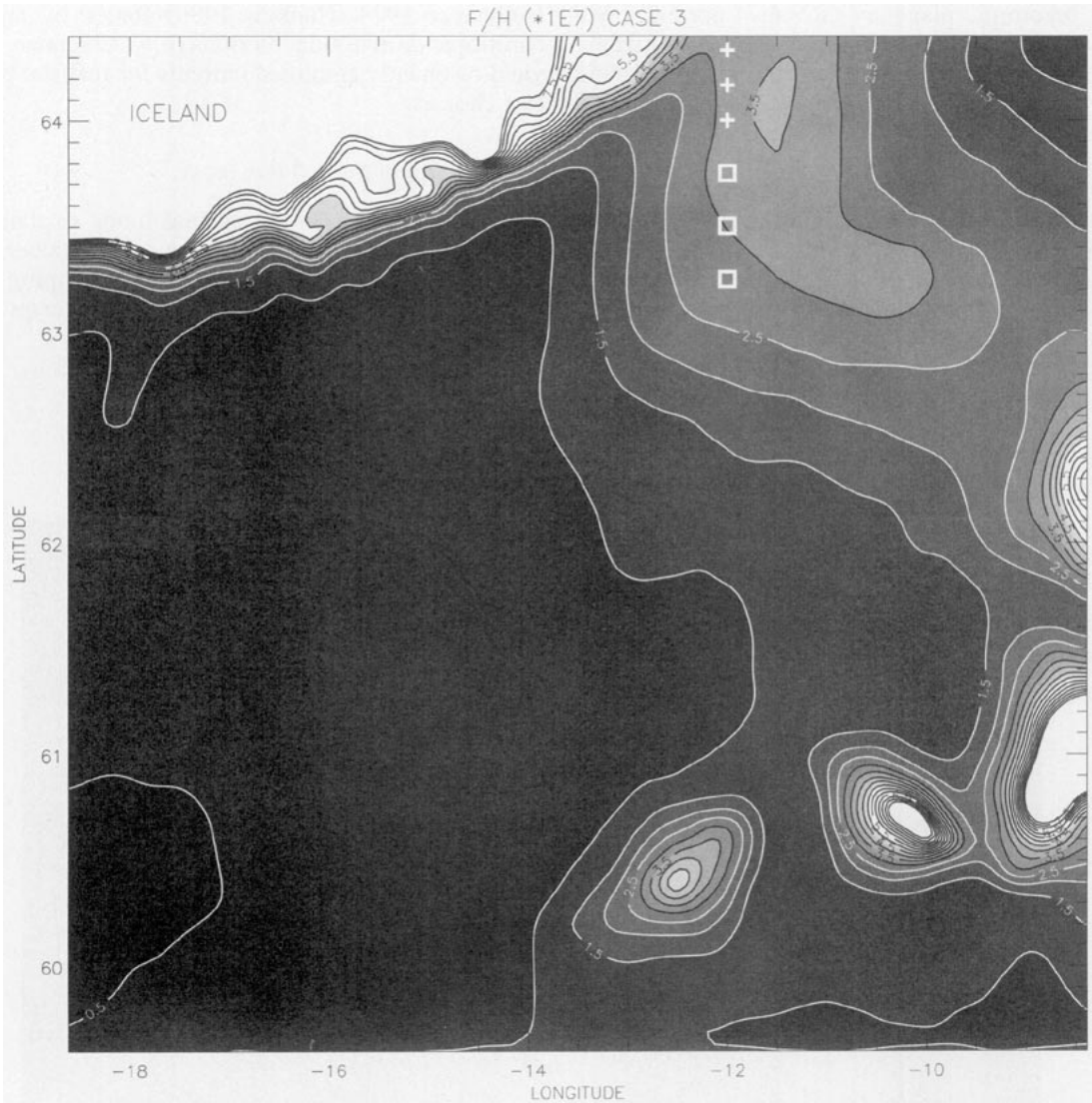

FIG. 6. *f/H* contours for case 2, from topography smoothed with a five-point (2–4–5–4–2) grid-scale filter. Plotted as in Fig. 1 but with central grid point (62°N, 13.5°W) and grid resolution 3.33 km.

width of the spectral peak at the half-power point. Using the eight spectra from moorings 1, 2, and 3 computed using the entire records (roughly 260 days), we obtain seven estimates of T_d (10, 9, 9, 7, 10, 8, and 9 days; the spectrum at 300-m depth of mooring 2 did not have a well-formed peak), which average to T_d = 8.8 days. If we instead compute spectra during the four intervals of strong excitation defined by the EOF coefficient time series, we obtain a somewhat longer damping time. We computed this for each of the seven subsampled spectra and found an average T_d = 13 days (from individual subsampled spectral estimates of 13, 13, 14, 12, 10, 12, and 15 days). This estimate of T_d should be more accurate than the former since it is evaluated from time periods when the oscillation is strongly excited, rather than over a long interval of infrequent excitation, which may result in fictitious broadening of the resonant peak. Note that the *e*-folding period for the modes is comparable to the time intervals of strong excitation as would be expected. Also note that these frictional decay time estimates are comparable with those invoked by Chapman (1989) in modeling the resonant response of topographic vorticity modes to diurnal tidal forcing. Specifically, Chapman (1989) used a linear velocity damping coefficient of the form γ/H with $\gamma = 5 \times 10^{-4}$; nominal depths of 400 m and 1000 m in the IFF then yield theoretical decay times of 9 and 23 days, respectively, which are in line with our direct observational estimates.

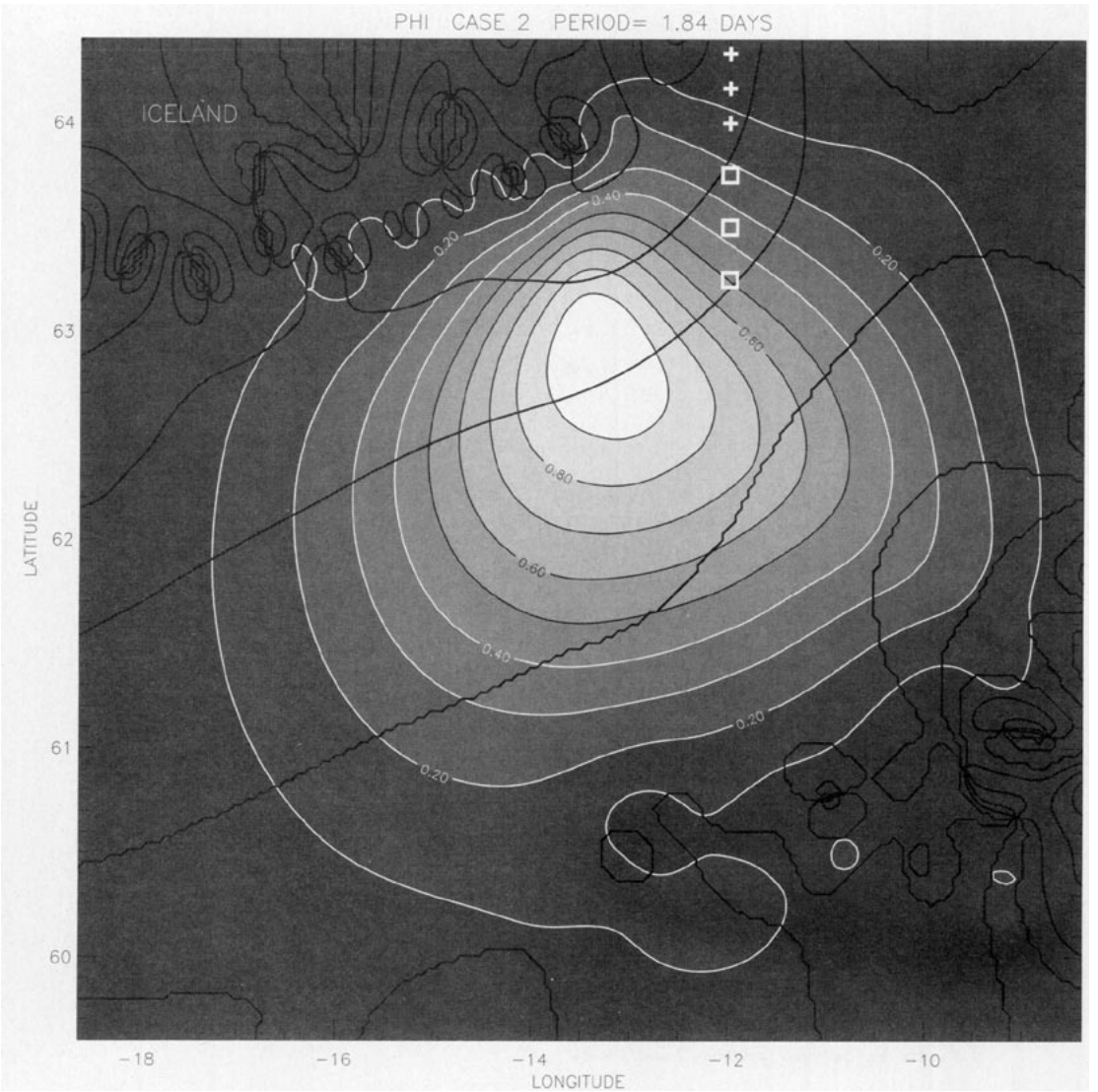

FIG. 7. Solution to (3) with period 1.84 days for the geometry of Fig. 6. Volume transport streamfunction is plotted (shaded contours amplitude, heavy lines phase in $\pi/4$ intervals). Grid resolution is 3.33 km.

It should be noted that there may be multiple modes contributing to the observed peak. This is because, as found by Miller (1986), a given large-scale mode can couple to smaller-scale topographic[2] modes forming a family of modes, the members of which each bear structures resembling the large-scale (uncoupled) counterpart but oscillate with a slightly different frequency. If such a family is stochastically excited to resonance, the resulting broadband peak will be broader than the broadband peak due to a single resonantly excited mode. An estimate of the frictional damping rate obtained from the broadband peak of a family of modes (assuming only one mode exists) will evidently be greater than the true frictional damping rate. Thus, in our case, frictional damping may actually be weaker than estimated above if such rending does occur. For example, in our numerical calculations here, members of the 1.8-day mode family tend to have periods between 1.75 and 1.95 days. If these modes are excited simultaneously in the presence of weak friction, they would form a peak at a mooring location with

[2] In some low-resolution calculations of the shallow-water normal modes of the Arctic/North Atlantic Ocean, using the techniques of Platzman et al. (1981), we also observed coupling between the Arctic Kelvin mode (period 1.86 days) and a poorly resolved topographic mode on the south side of the IFR. It would be surprising, however, if such coupling did occur in nature whereby energy leaks between the very large-scale Kelvin-like mode of the Arctic to a topographic–Rossby mode of the IFR.

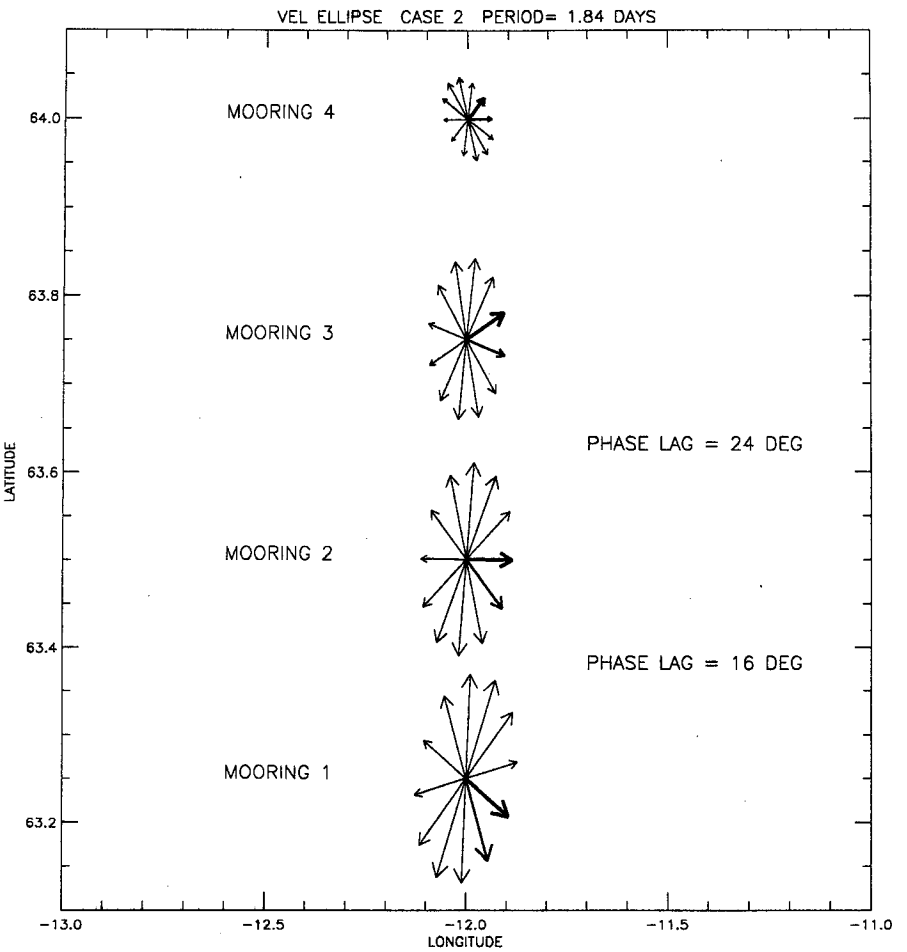

FIG. 8. Velocity ellipses for the normal mode shown in Fig. 7 at the locations of the current meter moorings 1 through 4. Rotation of the currents is anticyclonic as observed in Fig. 5. Dark arrow indicates zero phase angle for comparison among the three locations; phase lag between moorings 1 and 2 is 16° and between moorings 2 and 3 is 24°.

width dependent upon the local mode amplitudes, their frequencies, and their projections onto the forcing function. If all the computed family members strongly contribute to the observed peak, T_d would be roughly 17 days, a value comparable to our estimate of frictional decay time under the single-mode hypothesis. The simultaneous excitation of the members of such a family of modes is unresolvable by our data. However, a careful look at the spatial amplitude structures of the computed family members leads us to comment that it is more likely that only two or three of the family members can contribute strongly to the region around the current meter; based on the computed family members' intrinsic frequencies (with weak friction) an estimate of $T_d = 40$ days follows, which would yield a much narrower peak than was found in the data. Thus, our estimate of a frictional damping time $T_d = O(9-13)$ days is likely a real effect of friction.

c. *Forcing of the 1.8-day mode*

The primary candidate for forcing the observed barotropic normal mode resonance is atmospheric wind stress curl via Ekman pumping velocity at the base of the surface frictional layer (e.g., Gill 1982). Other potential forcing functions include atmospheric sea level pressure variations, Ekman divergence of longshore wind stress, radiation from instabilities of the Iceland–Faeroe frontal current, and topographic coupling with remote waves.

In order to study the importance of atmospheric forcing of the resonant normal mode, we obtained the National Centers for Environmental Prediction's 6-hour operational global data assimilation system surface wind stress and sea level pressure fields (White 1995; Roads et al. 1996, manuscript submitted to *J. Atmos. Sci.*), which were available on a 0.94° latitude–longi-

tude grid over the time interval of our observations. Wind stress curl was computed using centered differences on the 0.94° grid. We selected several key atmospheric grid points (e.g., nearest the current meters, upstream, downstream, and southward of moorings) and plotted time series of the raw atmospheric data. We found no suspicious activity, so the data was used in raw form. Inspection of the time series (not shown) of wind stress, wind stress curl, and sea level pressure variations reveal that during the previously identified strong excitation periods of the normal mode the atmospheric fields tend to exhibit variability with period near 2 days (and sea level pressure experiences a drop to lower values), which is consistent with an atmospheric forcing mechanism. The atmospheric fields are highly correlated over the spatial extent of the normal mode (61°S–64°N; 15°–10°W), so we additionally defined several averaging areas for the atmospheric fields (to eliminate smaller-scale noise and to identify bulk effects over the theoretically predicted spatial extent of the normal mode). Then we computed coherence between ocean currents at mooring 1 (80 and 300 m) and zonal wind stress, meridional wind stress, wind stress curl, and sea level pressure at the selected grid points and for the areal averages (subsequently defined). Coherences between the atmospheric variables and 80-m currents are virtually the same as those for 300-m currents, so only the former are discussed.

Our atmosphere–ocean coherence results are summarized as follows. Zonal wind stress is strongly coherent with both horizontal ocean velocity components in the relevant period band centered at 1.8 days, frequency 0.56 cpd (Fig. 9, circles). Peak coherence magnitude between zonal wind stress and zonal current reaches 0.8, while zonal stress and meridional current coherence magnitude tops 0.7. This applies for both a local area average of zonal stress around the moorings (62.8°–63.8°N; 13.1°–11.3°W) and an average over the entire spatial extent of the theoretical normal mode (60.9°–63.8°N; 15.0°–10.3°W). Meridional wind stress is not significantly coherent with zonal current in that band, but coherence magnitude exceeds 0.50 (just below the 95% significance level of 0.55) for meridional stress and meridional currents at 0.56 cpd in area averages around the moorings (e.g., Fig. 9, +). Wind stress curl is not significantly coherent with either zonal or meridional currents in the frequency bin (0.56 cpd) centered on the observed resonant peak (Fig. 9, ×). Wind stress curl is marginally coherent with meridional currents in the 0.53 cpd and 0.50 cpd frequency bands (low-frequency side of the resonant peak) but only for spatial averages computed over the bulk of the theoretical normal mode extent (e.g., Fig. 9, ×). Sea level pressure coherence with zonal velocity has a peak in magnitude at 0.45, which is below the 95% significance level; meridional velocity is not coherent with sea level pressure.

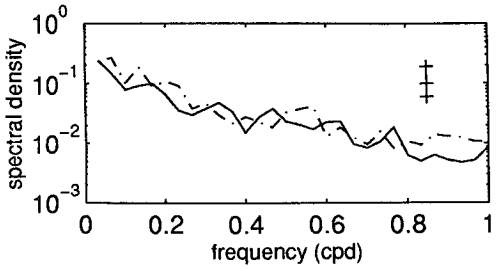

FIG. 10. Rotary spectrum of wind stress τ averaged over (62.8°–63.8°N, 11.3°–13.1°W). Cyclonic is solid, anticyclonic is dash–dotted, and 95% confidence limits are indicated.

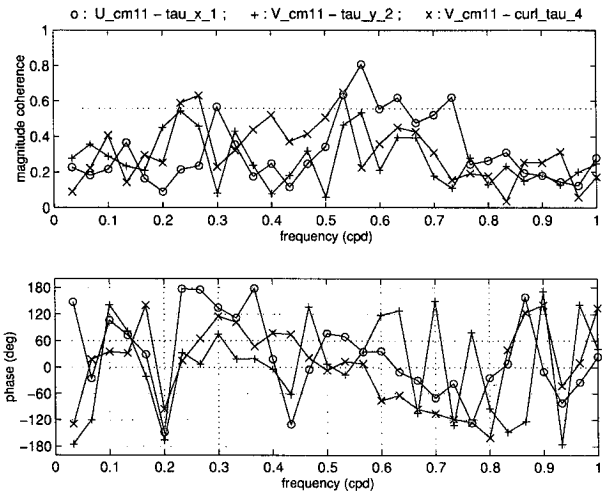

FIG. 9. Coherence spectra of 80-m currents at mooring 1 (63.25°N, 12°W) and atmospheric variables; (top) coherence magnitude, (bottom) coherence phase. Circles correspond to zonal current and zonal wind stress averaged over (62.8°–63.8°N, 11.3°–13.1°W), + correspond to meridional current and meridional wind stress averaged over (61.8°–62.8°N, 11.3°–13.1°W), and ×'s correspond to meridional current and wind stress curl averaged over (60.8°–63.8°N, 10.3°–15.0°W). The 95% level of significance for the coherence amplitude is indicated by the dotted line. Positive phase indicates that the first variable leads the second.

It next must be shown that the ocean response is not simply a nonresonant slave to atmospheric forcing. The anticyclonic wind stress has a weak but significant peak centered at 1.8 days in its rotary autospectrum (Fig. 10) over the current meter moorings. It is evident from comparison of Fig. 10 to Fig. 2 (N.B., the different ordinates) that the oceanic response is more narrow-banded than the atmospheric wind stress, which is indicative of a resonant (rather than static) ocean response. Also, the phase relation between zonal wind stress and the zonal ocean current changes by 87° as the frequency increases through the resonant peak from 0.50 to 0.63 cpd. This is consistent with a resonantly forced response wherein the driving signal leads the response by smaller values on the low-frequency side of the peak and larger values on the high-frequency

side. (For a simple harmonic oscillator, 0° and 180° phase are the limiting values at zero and infinite frequency, whereas in this case the spatial structure of the normal mode and that of the atmospheric forcing determine spatially dependent limiting values of phase that we have not theoretically predicted here.) Atmospheric cross-spectra were then used to identify a predominantly north-northeastward propagation direction for atmospheric wind stress disturbances in the relevant period band over the spatial extent of the theoretical normal mode. Since the theoretical normal mode phases propagate northwestward, the propagating atmospheric forcing overlaps the oceanic propagating signal in the northward direction and can thereby project significantly onto the northward propagating component of the normal mode. However, it must be noted that the moorings are oriented along a north–south line so we cannot distinguish from mooring data alone whether the east–west component of the propagating ocean response is in opposite direction (westward) to that of the atmospheric forcing (eastward), which would plainly indicate a dynamic (rather than static) ocean response. On the other hand, coherence phase calculations for zonal wind stress disturbances in the relevant period band show that they propagate northward at least three times faster than the oceanic phases propagate between the moorings, which is another strong indicator of a dynamic ocean response.

These results clearly reveal the atmosphere as the driving mechanism for a dynamic oceanic normal mode resonance but they leave unanswered questions regarding the precise mechanism of forcing. For example, it is unsatisfying to find that zonal wind stress correlates more strongly with the observed ocean response than does the wind stress curl. While this could be attributed to inaccuracies in estimating the true wind stress curl, it may be an indication of another type of forcing mechanism such as Ekman divergence of longshore wind stress along the southeast coast of Iceland combined with nearshore proximity of the theoretical vorticity mode. Energetic zonal wind stress events in the relevant frequency band may also trigger bursts of Rossby–topographic wave radiation from the unstable (and 50-km proximate) Iceland–Faeroe frontal current in a similar way that radiation of energy from unstable currents was shown by Miller et al. (1987) to excite basin-scale topographic–Rossby normal mode resonances in eddy-resolving general circulation models.

5. Summary

We have presented observational and theoretical evidence for the existence of a barotropic topographic–Rossby normal mode with period 1.8 days that is resonantly excited on the south side of the Iceland–Faeroe Ridge. A spatial array of current meter moorings reveals coherency over at least 55-km scales and barotropic phase propagation among moorings with shallower water on the right. The signal is sporadically excited with 4 cm s^{-1} rms velocity amplitude and decays with an amplitude e-folding timescale of approximately 13 days. The observed velocity field is coherent in the resonant period band with atmospheric zonal wind stress and marginally coherent with large-scale atmospheric wind stress curl. A rigid-lid shallow-water model predicts a barotropic topographic–Rossby normal mode with period near 1.8 days localized over the observed topography of the ridge. It has a spatial extent of over 250 km and is well matched to the observed phase lags between current meter moorings and to the observed features of the velocity ellipses. This appears to be the first clear evidence of a stochastically forced resonant barotropic topographic–Rossby normal mode in the ocean.

Acknowledgments. AJM is funded by ONR (N0014-96-0264), NOAA (NA36GPO372 and NA47GPO188), and the G. Unger Vetlesen Foundation. PFJL thanks SACLANT Undersea Research Centre for support and hospitality while a visiting summer student and is supported at Harvard under ONR Grant N00014-93-10577. This work began during PFJL's summer 1994 visit, while AJM and PMP were employed as scientists at SACLANT. We are grateful to Doug Luther for background references and an insightful review. John Roads generously provided us with the NCEP atmospheric analyses. We also thank Ken Brink, George Platzman, Stefano Pierini, and the anonymous referee for important comments on the manuscript, discussions, background information, and/or preprints of their work.

REFERENCES

Bendat, J. S., and A. G. Piersol, 1986: *Random Data, Analysis and Measurement Procedures.* John Wiley and Sons, 566 pp.

Brink, K. H., 1991: Coastal-trapped waves and wind-driven currents over the continental shelf. *Annu. Rev. Fluid Mech.*, **23,** 389–412.

Cannon, G. A., and D. J. Pashinski, 1990: Circulation near Axial Seamount. *J. Geophys. Res.*, **95,** 12 823–12 828.

——, ——, and M. R. Lemon, 1991: Middepth flow near hydrothermal venting sites on the southern Juan de Fuca Ridge. *J. Geophys. Res.*, **96,** 12 815–12 831.

Chapman, D. C., 1989: Enhanced subinertial diurnal tides over isolated topographic features. *Deep-Sea Res.*, **36,** 815–824.

Chave, A. D., J. H. Filloux, D. S. Luther, L. K. Law, and A. White, 1989: Observations of motional electromagnetic fields during EMSLAB. *J. Geophys. Res.*, **94,** 14 153–14 166.

Gill, A. E., 1982: *Atmosphere–Ocean Dynamics.* Academic Press, 662 pp.

Hopkins, T. S., 1991: The GIN Sea. Review of physical oceanography and literature from 1972. *Earth Sci. Rev.*, **30,** 175–318.

Hunkins, K., 1986: Anomalous diurnal tidal currents on the Yermak Plateau. *J. Mar. Res.*, **44,** 51–69.

Huthnance, J. M., 1974: On the diurnal tidal currents over Rockall Bank. *Deep-Sea Res.*, **21,** 23–35.

Luther, D. S., 1982: Evidence of a 4–6 day planetary oscillation of the Pacific Ocean. *J. Phys. Oceanogr.*, **12,** 644–657.

——, 1995: Waves trapped to discrete topography: Existence and implications. *Proc. Eighth Hawaiian Winter Workshop,* P. Mul-

ler and D. Henderson, Eds., University of Hawaii at Manoa, 43–56.

Miller, A. J., 1986: Non-divergent planetary oscillations in midlatitude ocean basins with continental shelves. *J. Phys. Oceanogr.*, **16,** 1914–1928.

——, 1989: On the barotropic planetary oscillations of the Pacific. *J. Mar. Res.*, **47,** 569–594.

——, W. R. Holland, and M. C. Hendershott, 1987: Open-ocean response and normal-mode excitation in an eddy-resolving general circulation model. *Geophys. Astrophys. Fluid Dyn.*, **37,** 253–278.

Niiler, P. P., S. Piacsek, L. Neuberg, and A. Warn-Varnas, 1992: Sea-surface temperature variability of the Iceland–Faeroes Front. *J. Geophys. Res.*, **97,** 17 777–17 785.

Perkins, H., 1992: Large-scale structure of the Iceland–Faeroe Front. SACLANT Undersea Research Centre Rep. SR-189, La Spezia, Italy, 40 pp. [Available from SACLANTCEN, Viale San Bartolomeo, 400, 19138 La Spezia, Italy.]

Pierini, S., 1996: Topographic Rossby modes in the Strait of Sicily. *J. Geophys. Res.*, **101,** 6429–6440.

Platzman, G. W., 1975: Normal modes of the Atlantic and Indian Oceans. *J. Phys. Oceanogr.*, **5,** 201–221.

——, G. A. Curtis, K. S. Hansen, and R. D. Slater, 1981: Normal modes of the world ocean. Part II: Description of modes in the period range 8–80 hours. *J. Phys. Oceanogr.*, **11,** 579–603.

Poulain, P.-M., A. Warn-Varnas, and P. P. Niiler, 1996: Near surface circulation of the Nordic Seas as measured by Lagrangian drifters. *J. Geophys. Res.*, **101,** 18 237–18 258.

Rhines, P., and F. Bretherton, 1973: Topographic Rossby waves in a rough-bottomed ocean. *J. Fluid Mech.*, **61,** 583–607.

Roads, J., S.-C. Chen, M. Kanamitsu, and H. Juang, 1996: GDAS' GCIP Energy Budgets. *J. Atmos. Sci.*, in press.

Saint-Guily, B., and A. Lamy, 1988: Ondes guidées par le talus de l'île de Kerguelen. *C. R. Acad. Sci. Ser. II: Mec. Phys. Chim. Sci. Terr. Univers.*, **307,** 573–578.

White, G., 1995: An intercomparison of precipitation and surface fluxes from operation NWP Analysis/Forecast Systems. WMO/ICSU/IOC Rep. No. 22, 165 pp. [Available from Joint Planning Staff for WCRP, c/o World Meteorological Organization, Case Postale No. 2300, CH-1211 Geneva 2, Switzerland.]